ChemPubSoc Europe

DOI: 10.1002/celc.201800532

CHEMELECTROCHEM Articles

Electrocatalytic Study of the Thin Metallopolymer Film of [2,2′-{1,2-Ethanediylbis[Nitrilo(1E)-1-Ethyl-1-Ylidene]}Diphenolate]-Nickel(II) for Ethanol Electrooxidation

André Olean-Oliveira,[a] Camila F. Pereira,[a] Diego N. David-Parra,[a] and Marcos F. S. Teixeira*[a]

The present paper describes the electrochemical activity of a Ni(II)-Schiff base metallopolymer electrode for the oxidation of ethanol in alkaline media. The scanning electron microscope results show that the metallopolymer at the glassy carbon surface has a nanoflake-like lamellar structure, and there is no molecular structural change after treatment with NaOH. Voltammetry measurements indicate that the metallopolymer acts as efficient material for the electrocatalytic oxidation of ethanol, where a high-valent nickel(IV) was revealed as the reactive intermediate during the anodic scan. An isopotential point can be observed in rotating disk electrode voltammetry for ethanol oxidation. The electrode surface may be considered to consist of two independent electrochemical regions, one corresponding to the ethanol electro-oxidation by nickel(IV) and the second corresponding to water oxidation. The Tafel slopes were found to be 246 mV dec^{-1} at low overpotentials and 44 mV dec^{-1} at high overpotentials, which suggest that the first electron transfer step is the rate controlling step. The specific activity of the metallopolymer-modified electrode for the ethanol electro-oxidation reaction was 6.66 mA cm^{-2} for 0.130 μmol cm^{-2} of electroactive species of metallopolymer at 0.6 V vs. SCE.

1. Introduction

The study of metallopolymers has been intensively applied, with new strategies found in π-conjugated polymers.[1] The metal-containing polymers emerged through research aimed at merging the versatility of conducting polymers and the highly efficient redox conductivity of transition metals, resulting in π-conjugated polymers with redox-active metal centers with interesting chemico-physical properties.[2] These materials are highly useful in a wide range of applications, such as catalysts[3] and photocatalysts.[4]

Among the metallopolymers reported in the literature, the poly[metal(salen)] is a relatively new class of nanopolymers[5] that are being studied due to their electrochemical and electrocatalytic properties.[6] The tetradentate N_2O_4 salen moieties form stable complexes with metals of different oxidation states and 3D molecular architectures. Many of these polymer network structures are more active centers than only the complexes. The poly[metal(salen)] not only provides a catalytic activity but also facilitates electron transfer through the conjugated polymer chain as the backbone. The linkage existing between the dπ orbitals of metal centers and π or π* orbitals of the conjugated polymer induces the electron transfer.[7] Therefore, it is of interest to study the electrocatalytic activity of these polymers. In our research group, we have investigated the formation of multiblock poly[metal(salen)] by electropolymerization[7a,8] and its application as electrocatalysts.[9] The metallopolymers tend to be organized as molecular columns, forming a π-conjugated multiblock system due to the interaction of the metal center with the aromatic ring of the adjacent molecule.[10]

The electro-oxidation of ethanol in alkaline medium is usually studied with metal nanoparticles,[11] a metal composite,[12] nanometal supported on carbon,[13] or nanometal supported on polymer,[14] and therefore, these materials find potential applications in fuel cells. However, the kinetics of ethanol electro-oxidation are slow and produce different intermediates, reducing the electrocatalytic efficiency and lifetime of the metal. One of the alternatives to minimize these effects would be the use of metallopolymer complexes.

In this communication, we present the results of a study on the electrocatalytic oxidation of ethanol on the Ni(II)-Schiff base metallopolymer-modified glassy carbon electrode. Experiments were performed in alkaline solution, and electrochemical characterization was carried out by cyclic voltammetry, chronoamperometry, rotating disk electrode voltammetry and impedance spectroscopy.

Experimental

Synthesis of the [**2,2′-{1,2-Ethanediylbis[Nitrilo(1E)-1-Ethyl-1-Ylidene]}Diphenolate**]-Nickel(II) Complex ([Ni(α,α′-Methyl$_2$Salen)])

The ligand **2,2′-{1,2-ethanediylbis[nitrilo(1E)-1-ethyl-1-ylidene]}-diphenol** (α,α′-methyl$_2$salen) **was purchased from Sigma Aldrich** and used without further purification. The metallic complex [Ni(α,α′-methyl$_2$salen)] (Figure 1) was prepared by the addition of stoichiometric and equimolar amounts of the *Schiff* base ligand and nickel acetate (Sigma-Aldrich) in absolute ethanol. The solution

[a] *A. Olean-Oliveira, C. F. Pereira, Dr. D. N. David-Parra, Prof. M. F. S. Teixeira*
Department of Chemistry and Biochemistry
School of Science and Technology
Sao Paulo State University (UNESP)
Rua Roberto Simonsen, 305
CEP 19060-900 - Presidente Prudente, SP, Brazil
Fax: + 55 18 3221 56 82
E-mail: marcos.fs.teixeira@unesp.br

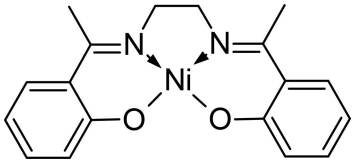

Figure 1. Molecular structure of the [Ni(α,α′-methyl$_2$salen)] complex.

was kept under reflux for 3 h at 50 °C with constant stirring to yield a red precipitate. The precipitate was filtered in a Gooch crucible, washed with absolute ethanol and kept in a desiccator. FTIR (ν cm^{-1}) in KBr: 3339, –OH_{ph}; 1612, C=N; 1505, C=C; 1291, >C–O_{ph}; 1023, ring breathing; and 501, Ni–O. UV-*vis* (nm) in CH_3CN: 250 (π→π*); 326 (π→π*); 403 (n→π*); and 547 (MLCT).

Electrosynthesis of Poly[Ni(α,α′-Methyl$_2$Salen)]

The electrosynthesis was performed in a conventional electrochemical cell with three electrodes including the following: a saturated calomel electrode (SCE) as the reference electrode, a platinum wire electrode as the auxiliary electrode and a glassy carbon electrode (GC) (A = 0.071 cm^2), which were connected to a potentiostat/galvanostat μ-Autolab type III (Eco Chimie). The polymer film was formed by electropolymerization using 1.0 mmol L^{-1} of the [Ni(α,α′-methyl$_2$salen)] complex in acetonitrile (Sigma Aldrich 99.9%) with tetrabutylammonium perchlorate (PTBA) (Sigma-Aldrich) electrolyte at a concentration of 0.10 mol L^{-1} while applying a potential range of 0.0 to 1.4 V vs. SCE at 100 mV s^{-1} in a N_2 atmosphere.

Electrochemical Behavior

The activation of the modified electrode for the electrocatalysis of ethanol oxidation was performed by cycling the potential in 0.10 mol L^{-1} NaOH in a potential range of 0.0 to 0.8 V vs. SCE. The electrocatalytic activity from the ethanol oxidation reaction was generated by the application of potentials through cyclic voltammetry using a potential range of 0.0 to 0.8 V vs. SCE at a scan rate of 50 mV s^{-1}.

Electrochemical impedance measurements were performed with Palsens3 interfaced PSTrace 5.2 software. A sinusoidal voltage perturbation with an amplitude of 10 mV rms was applied in the frequency range between 50 kHz and 0.01 Hz with 10 frequency steps per decade. EIS measurements were performed in 0.5 mol L^{-1} KCl solution before and after activation of the modified electrode with NaOH. Fitting of the spectra with the equivalent electrical circuits was performed with EIS Spectrum Analyser 1.0 software.

Rotating disk electrode voltammetry (RDEV) was conducted with a μ-Autolab type III (Eco Chimie) connected to a microcomputer and controlled by GPES software. RDE measurements were performed with a motor speed controller (Autolab RDE, Eco Chimie). The GCE electrode modified with metallopolymer (diameter 3.0 mm) was rotated between 500 and 2500 rpm using 0.1 mol L^{-1} ethanol in 0.1 mol L^{-1} NaOH. For the chronoamperometric analysis, a constant potential of 0.6 V was applied for 3000 s at the modified electrode immersed in 0.1 mol L^{-1} NaOH solution containing 0.1 mol L^{-1} ethanol.

Morphological Characterization

The surfaces of the metallopolymer-modified electrode were examined using an EVO 50EP (Carl Zeiss SMT AG, Germany) scanning electron microscope (SEM). All observations were carried out with a secondary electron (SE) detector in high-vacuum mode at an accelerating voltage of 15 kV. Raman spectroscopy measurements were obtained with a Renishaw Raman spectrometer with laser at an excitation wavelehgth of 663 nm and a diffraction grating of 1800 lines per millimeter. The exposure time was set at 10 s with three accumulations.

2. Results and Discussion

2.1. Electrochemical Characterization

The electrodeposition of the metallopolymer film on conductor substrate is illustrated in Scheme 1. Typically, the anodic oxidation of metal-salen complexes on the electrode generate

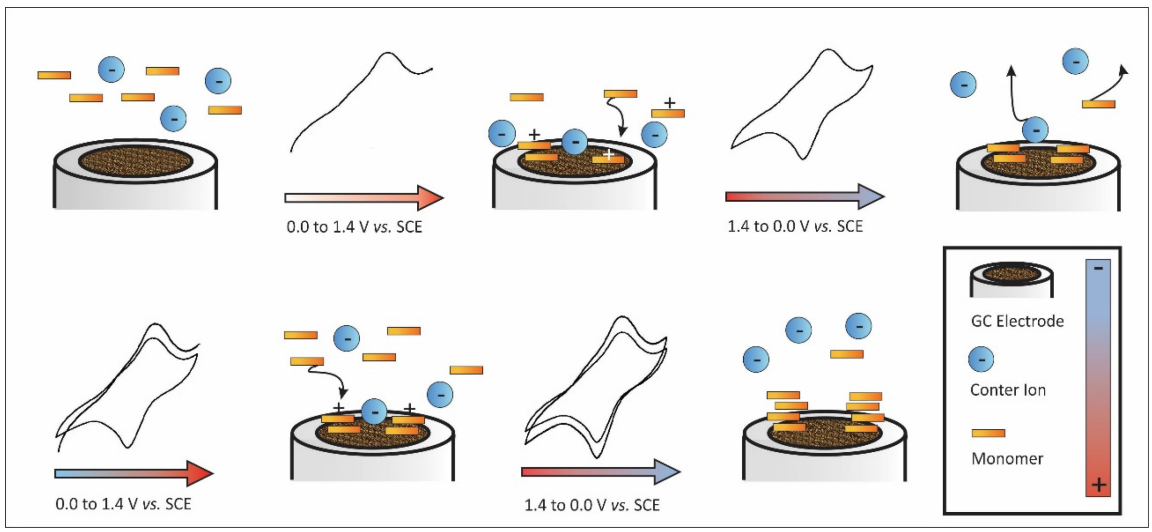

Scheme 1. Polymer organization of the metallopolymer on the conductor substrate. Monomer = [Ni(α,α′-methyl$_2$salen)] complex; Counter ion = perchlorate anion.

electron-deficient metal centers, and the electropolymerization process occurs by interactions of the electron-rich π system of the adjacent complex with electron-deficient cation-radicals functioning as bridges between the molecules.[7a,8,9c,15]

Figure 2 shows that successive scans produce an increase in both the anodic and cathodic peak currents. The positive

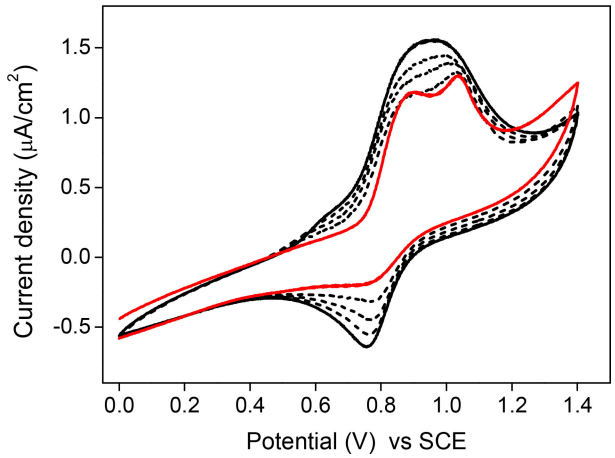

Figure 2. Cyclic voltammograms for the electropolymerization of the [Ni(α,α′-methyl$_2$salen)] complex (1.0 mmol L^{-1}) on the glassy carbon electrode in acetonitrile containing 0.10 mol L^{-1} tetrabutylammonium perchlorate at a scan rate 100 mV s^{-1}.

potential limit of +1.0 V vs. SCE is required for the formation of cation radicals, which initiate the polymerization process.[9c] With the increase in scan number, the redox system becomes more evident, indicating continuous electrodeposition of the film onto the surface of the GC electrode. This fact suggests that the process approaches reversibility, which can also be deduced by the minimal shift of the peak potentials. The potential region between +0.75 to +0.85 V is related to the redox activity of Ni(II)/Ni(III) of the generated metallopolymer.

The formation mechanism of the polymeric film on the conductor surface can be ascribed to the interaction between *d*-orbitals of the metal centers with π-orbitals of aromatic rings of adjacent monomers, which enables easier electronic communication between the nickel centers in the conjugated backbone. The polymer organization is pre-established by insertion of the counter-ion from the supporting electrolyte[16] as charge balance into the positively charged structures that form the metallopolymer columns. The coverage of the metallopolymer on the GC was confirmed by the linear dependence of the anodic and cathodic peak currents with the potential scan rates (10 to 200 mVs^{-1}). This shows that the redox processes are controlled by an adsorption mechanism on the conductor surface and considered to be a Nernstian reaction. The concentration of the electroactive species of metallopolymer (0.130 μmol cm^{-2}) on the electrode surface was calculated from the linear slope of the plot of peak current as a function of the scanning rate. Under the electropolymerization conditions described above and assuming that the molar volume is equal to 267.6 (±7.0) cm^3 mol^{-1} (predicted data was generated using the ACD/Labs Percepta Platform), the film thickness of the resulting membrane was approximately 0.348 μm.

It is necessary to emphasize that previous to the electrocatalysis measurements, the metallopolymer film needed to be submitted to voltammetry cycling in sodium hydroxide medium. Initially, the metallopolymer-modified electrode was submitted to 50 cycles of potential scanning between 0.0 V and +0.8 V vs. SCE (see Figure 3A).

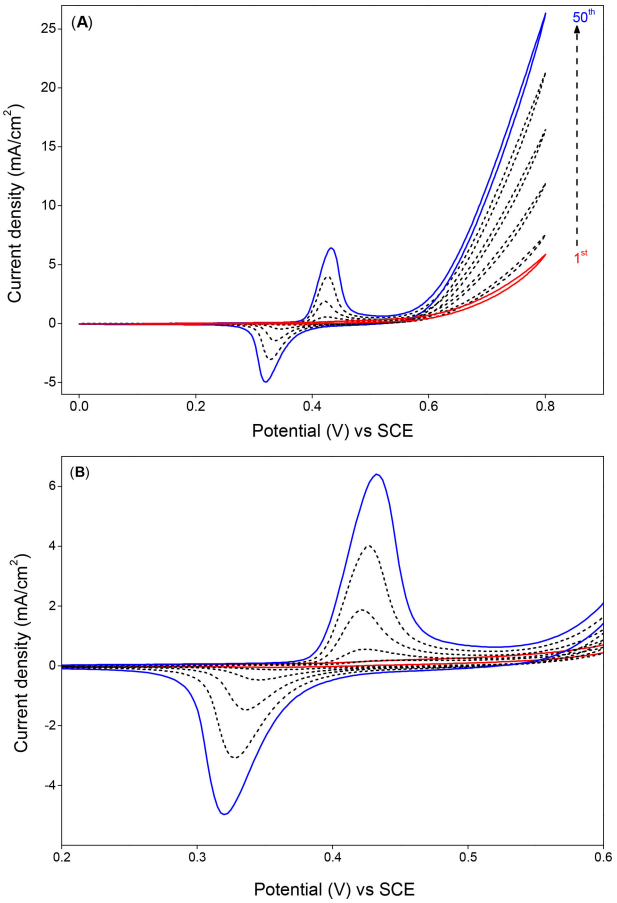

Figure 3. A) Cyclic voltammograms for activation of the poly[Ni(α,α′-methyl$_2$ salen)] in 0.10 mol L^{-1} NaOH alkaline medium applying 50 potential cycles at a scan rate of 50 mV s^{-1}. B) Magnification of the cyclic voltammograms.

The successive scans show several significant redox features apart from the oxygen evolution reaction (initially +0.6 V vs. SCE) in alkaline electrolyte. The voltammograms illustrate a continuous increase of the peak current intensities ($Ni^{(II/III)}$ redox process in the polymer structure), indicating a progressive activation of the metallopolymer in alkaline medium. The electrochemical processes related to the modified electrode were stabilized after fifty potential cycles. The cathodic and anodic peak potentials shifted to more negative/positive potentials, respectively, with an increase in the number of scans (Figure 3B). This is an indication of an increase in the electrical resistance of the polymer film. The resistivity changes and interface properties of the electrode surface were studied by electrochemical impedance spectroscopy.

Figure 4 shows the results of electrochemical impedance spectroscopy of the metallopolymer-modified electrode before and after treatment with NaOH. The impedance spectra were obtained at +0.45 V vs. SCE in an electrolytic solution of 0.5 mol L^{-1} potassium chloride.

The data were analyzed using an equivalent circuit containing four circuit elements, a solution-phase resistance (R_Ω), a constant phase element (CPE_1) in parallel with a charge transfer resistance (R_{ct}) and a second CPE_2 (see Figure 4C). The analyzed results are given in Table 1.

According to the Nyquist plot, a semicircular area with a R_{ct} of approximately 321.6 Ω cm^2 (Figure 4B red square curve) was obtained for the metallopolymer-modified electrode. After activation in alkaline medium, the value of R_2 increased to 676.6 Ω cm^2 (Figure 3B orange circle curve). The semicircle diameter corresponds to the electron transfer resistance of the nickel(II/III) process in the polymer structure. Therefore, the increase in electron transfer resistance was due to the insertion of the hydroxide anions on the positively charged structures between metallopolymer columns during successive anodic scans. This behavior collaborates the formation of a stacked structure of nickel-oxo-nickel bridges[17] interconnecting the metallopolymer columns. The CPE_2 element corresponds to a Warburg element, which is responsible for the diffusional control of the system at low frequency (<1 Hz). According to Bisquert,[18] the origin of the CPE_2 may be related to structural disorder effects, which yield distributions of microscopic hopping rates for ion diffusion.

The apparent electron transfer rate (k_{ET}) for the nickel redox reaction in the metallopolymer was determined using Equation (1):[19]

$$k_{ET} = \frac{1}{2R_{ct}CPE_2} \quad (1)$$

The k_{ET} values obtained were 1.00 s^{-1} and 0.42 s^{-1} at the metallopolymer-modified electrode before and after the potential cycling in NaOH, respectively. The trend in the electron transport kinetics seen in the redox process is to decrease in

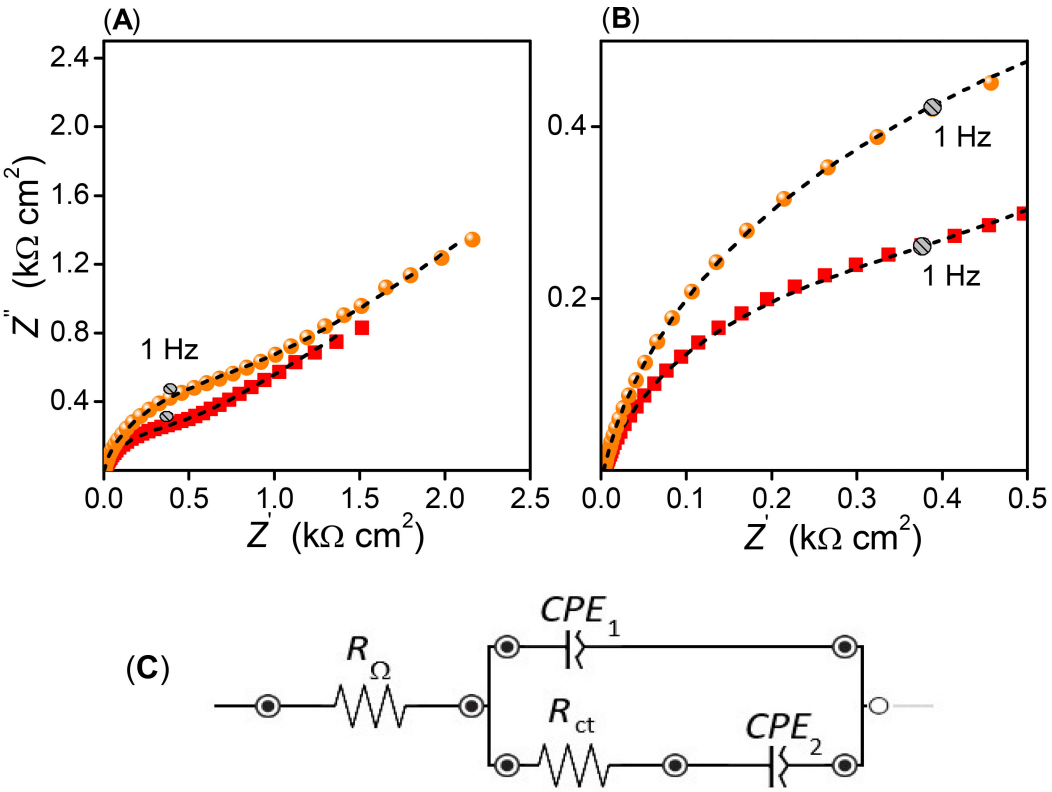

Figure 4. A) Complex plane impedance spectra recorded at the metallopolymer-modified electrode in 0.5 mol L^{-1} KCl at +0.45 V vs. SCE. **B**) Magnification of the high frequency part of the impedance spectra. Red square curve (■) = before treatment with NaOH; Orange circle curve (•) = after treatment with NaOH. The dotted lines show fitting to the electrical equivalent circuits in (**C**). Impedance spectra were recorded from 50 kHz to 0.01 Hz frequencies per decade with a sinusoidal amplitude of 10 mV.

Table 1. Fitted parameters of the electrochemical impedance spectra of the metallopolymer-modified electrode before and after potential cycling in NaOH.

	R_Ω [Ω cm^2]	CPE_1 [μF $s^{\alpha-1}$ cm^{-2}]	α_1	R_{ct} [Ω cm^2]	CPE_2 [mF $s^{\alpha-1}$ cm^{-2}]	α_2
before	4.16 ± 0.13	170.4 ± 6.8	0.82	321.6 ± 19.3	1.56 ± 0.08	0.45
after	3.95 ± 0.12	211.3 ± 7.2	0.87	676.6 ± 40.6	1.76 ± 0.06	0.50

sodium hydroxide solution. However, the electrocatalysis of alcohols is ideal in alkaline medium.

The morphology of the surface was analyzed by scanning electron microscopy to verify molecular structural change during the activation of the modified electrode. Figures 5A and 5B present images of the metallopolymer-modified electrode before and after treatment with NaOH, respectively.

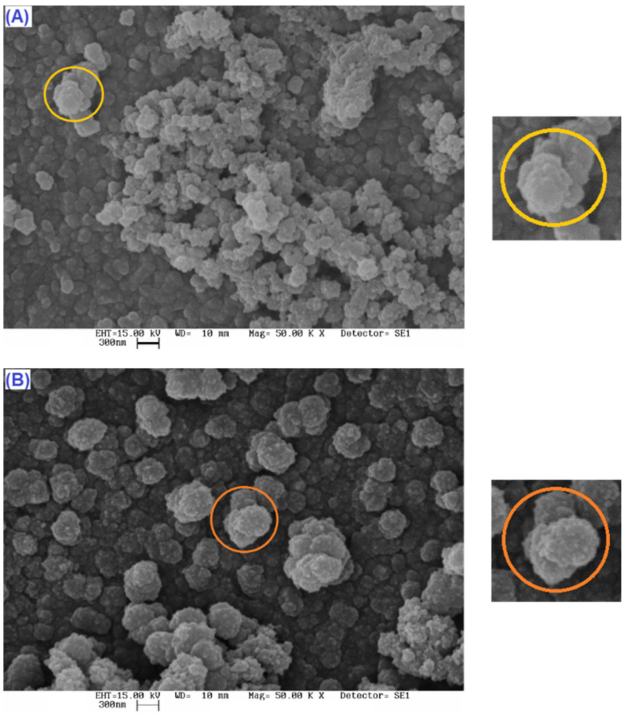

Figure 5. Scanning electron microscopy of the metallopolymer before (**A**) and after (**B**) the treatment with NaOH. The scale bar is 300 nm.

In both cases, the metallopolymer presents thin random stacked columns (irregular topography). As shown in the magnified images, the top end of these columns has a flake-like lamellar structure signifying that these columns grew along the axis. The stacked lamellar structures appear to have a nearly uniform average diameter of 150–450 nm. The presence of donor-acceptor interactions (metal-π system) stabilizes the intercalation of the metallo-complex, resulting in the stacking of molecules on the electrode surface. From these images, it is clear that the surface of the electrode was coated with conducting metallopolymers, and there is no morphological structure change of the electrode surface after treatment with NaOH. The EDS microanalysis is further performed to investigate the elementary composition of the electrode surface. The relative amounts of Ni (3.0%), C (50.4%), O (21.7%) and N (24.8%) were obtained for electrode before activation in alkaline medium. After activation, the relative amounts were of 1.8% Ni, 43.6% C, 26.6% O and 28.2% N. The small changes in C, O and N contents in the electrode after activation reveals that the chemical composition of the metallopolymer has not undergone a significant change. There was only a decrease in the percentage of nickel after the modified electrode was activated in alkaline medium.

The metallopolymer-modified electrodes was analyzed by Raman spectroscopy. Figure 6 presents the Raman spectra

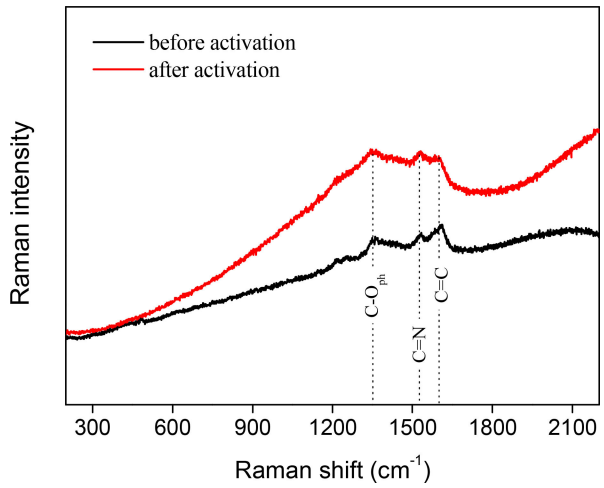

Figure 6. Resonance Raman spectra of the metallopolymer (black line) before and (red line) after the treatment with NaOH. $\lambda_{ex} = 663$ nm.

(excitation 633 nm) of the metallopolymer-modified electrode before and after treatment with NaOH. Analyzing the rotational and vibrational structures in the spectra, one can observe that the common bands associated the stretching of C–O_{ph}; C=N and C=C bonds in the 1600–1300 cm^{-1} region are very little affected after activation in alkaline medium. Another important aspect observed in the spectra is the strong of the fluorescence background after activation in alkaline medium. It is known that Schiff base complexes are fluorogenic materials and that fluorescence emission occurs with laser activation due to resonance between the emission bands of the complex. This increase fluorescence clearly indicates that the complex layer absorbed more the light of the excitation laser.

Recently, Kuznetsov and collaborators[20] studied electrochemical transformation of polymers based on nickel-salen in alkaline medium and in which they affirm the formation of nickel hydroxide thin film deposited on the surface electrode. Synthesis of the metallopolymer was carried out by potentiostatic electropolymerization at constant potential with cut-off of the charge passed. Comparing with our results, it is possible to verify morphological differences by characterization images. Apparently, the molecular structure of the polymer differs from that obtained by cycling the potential technique.

3.2 Electrocatalytic Alcohol Oxidation

To verify the electrocatalytic activity of the metallopolymer-modified glassy carbon electrode, the cyclic voltammograms were obtained in the absence and presence of ethanol in sodium hydroxide, as shown in Figure 7A. With the addition of ethanol in solution, the anodic current of the modified

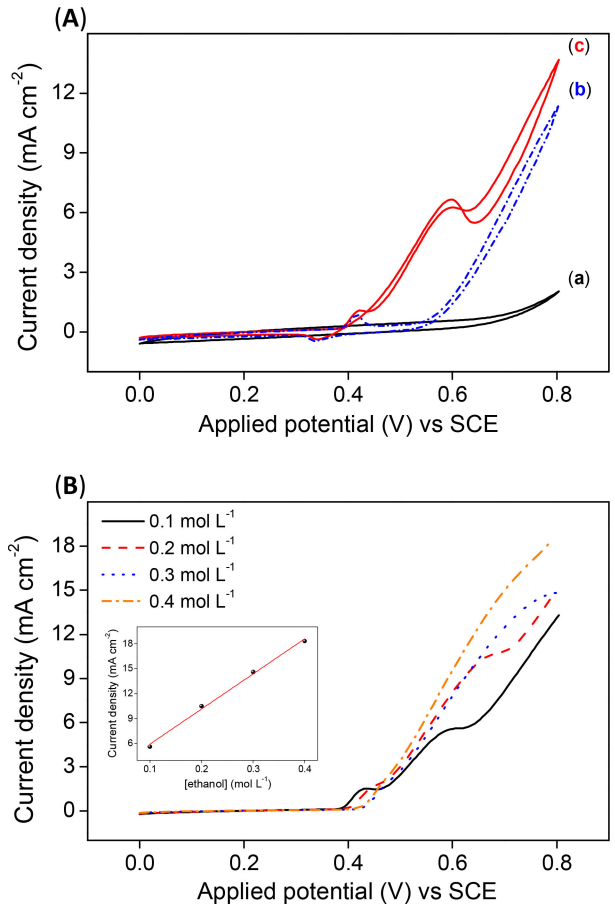

Figure 7. A) Cyclic voltammetric response obtained for the GC electrode in 0.1 mol L^{-1} NaOH solution containing 0.1 mol L^{-1} ethanol (black line, curve a); metallopolymer-modified electrode in 0.1 mol L^{-1} NaOH solution (blue dash dot, curve b); and metallopolymer-modified electrode in 0.1 mol L^{-1} NaOH solution containing 0.1 mol L^{-1} ethanol (red line, curve c). Scan rate = 50 mV s^{-1}. B) Voltammetric response for the metallopolymer-modified electrode in 0.1 mol L^{-1} NaOH solution containing 0.1 mol L^{-1} (black line); 0.2 mol L^{-1} (red dash); 0.3 mol L^{-1} (blue dot) and 0.4 mol L^{-1} (orange dash dot) of ethanol. Scan rate = 50 mV s^{-1}. Insert: anodic current density versus ethanol concentration.

electrode (see curve c of Figure 7A) increased significantly as well as exhibited a significant decrease in the overpotential of the oxidation reaction in comparison to an unmodified GC electrode (curve a). This behavior clearly indicates that the presence of the metallopolymer on the electrode surface significantly enhances the efficiency of the ethanol electro-oxidation process. The reverse scan peak is associated with the removal of intermediate species that were not completely oxidized in the direct scan.

On the basis of the experimental observations, it is likely that there is the formation of an unusual high-valent nickel(IV) (next at 0.59 V vs. SCE) as a reactive intermediate during the anodic scan. This can be observed in the voltammogram (curve c in Figure 7A), where the redox processes Ni(II)/Ni(III) (0.31–0.44 V vs. SCE) are kept at the same potential range as the voltammogram obtained in the absence of alcohol (curve b). Some authors have also suggested that over-oxidation causes Ni(IV) to form in alkaline medium.[21] Analyzing the Pourbaix diagram[22] suggests that there should be a Ni(III)/Ni(IV) reaction at approximately 200 mV above the Ni(II)/Ni(III) reaction at alkaline pH. Interestingly, the potential difference between the redox processes observed in the voltammogram (curve c) is equivalent in the prediction of the diagram. The distinct anodic peak in sodium hydroxide electrolyte can be treated as the chemisorption and oxidation kinetics of ethanol. These results corroborate with the observations of Nam and Cheng,[23] who studied the electrocatalytic property of a Ni (cyclam)-BTC network in alkaline medium, which was strongly relevant to the Ni(III)/Ni(IV) redox reaction activated by the potential dynamic process.

Furthermore, we investigated the effect of ethanol concentration on the modified electrode response. Figure 6B depicts linear voltammograms in 0.1 mol L^{-1} NaOH solution in the presence of various concentrations of ethanol (0.1–0.4 mol L^{-1}). Expectedly, peak potentials shift to more positive potential and the anodic current density increases as the ethanol concentration increased. In the insert of Figure 6B, the electrocatalytic peak currents are linearly dependent on the ethanol concentration. It is concluded that the mechanism of ethanol oxidation at the surface electrode may be ECE process. The voltammetric response of the metallopolymer-modified glassy carbon electrode for ethanol can be based on two redox steps in the electrocatalytic mechanism. The first step involves the electrochemical oxidation of nickel(II) in the polymer structure producing nickel(III), followed by the formation of the oxo bridges between metallopolymer columns. This is followed by the electron transfer of the ethanol and consequently regeneration of the nickel(II) in the metallopolymer. The second step is the electro-generation of nickel(IV) with the formation $Ni^{(IV)}$=O and subsequently the electro-oxidation of the intermediate species on the metallopolymer. Our proposal for the chemical and electrochemical processes is illustrated in Scheme 2.

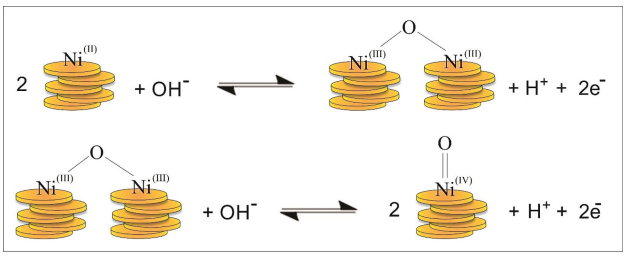

Scheme 2. Idealized chemical and electrochemical processes that occur at the metallopolymer on the electrode.

The influence of the mass-transport on the ethanol electro-oxidation was investigated by means of rotating disk electrode (RDE) voltammetry. The RDE voltammograms obtained using the metallopolymer-modified glassy carbon electrode with various rotation rates of 500 to 2500 rpm at scan rate of 25 mV s^{-1} are shown in Figure 8A. The RDE voltammograms obtained illustrate the complexity of ethanol electro-oxidation, with the rate-determining step on the nickel sites of the metallopolymer. It can be observed that the current density in

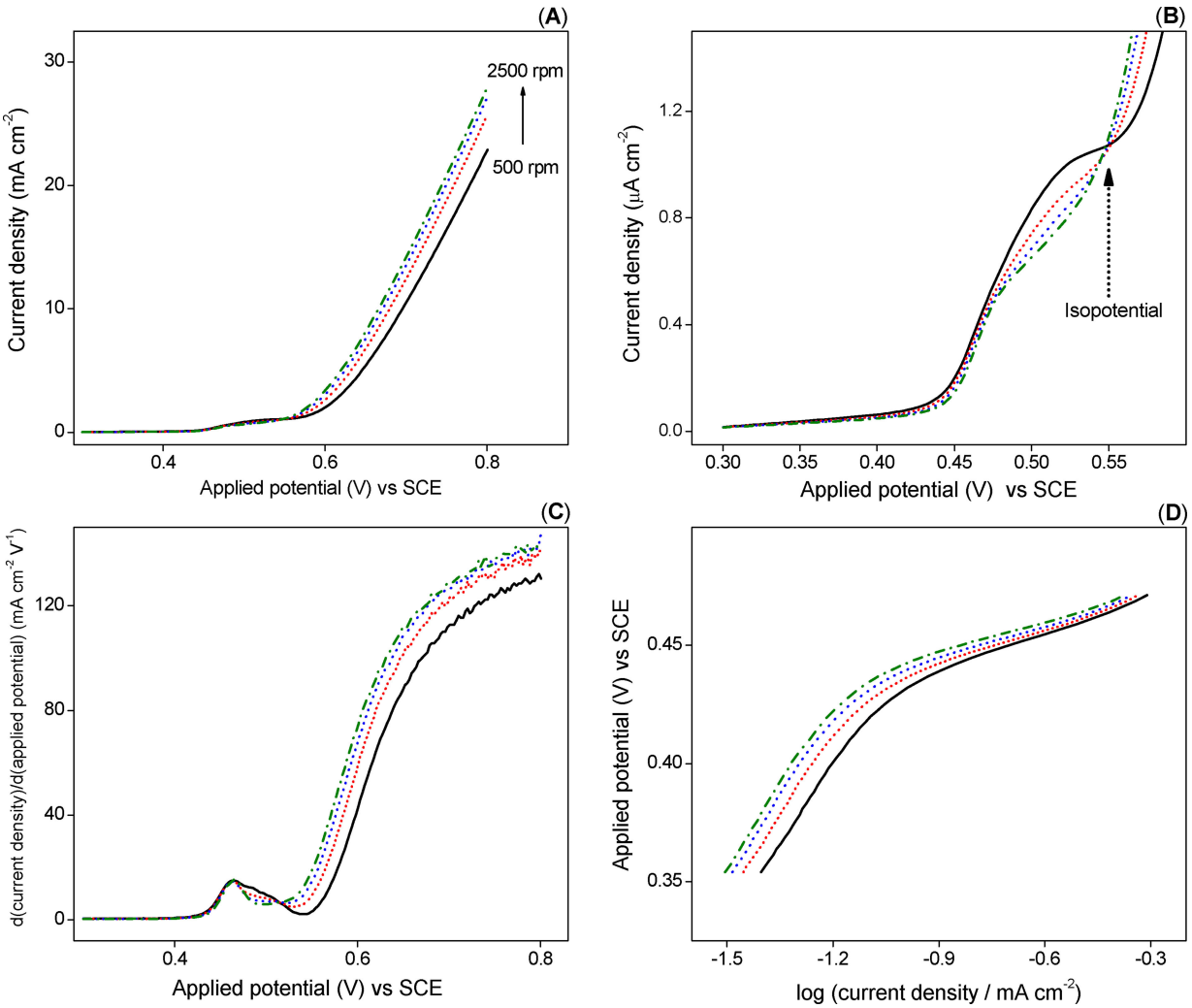

Figure 8. A) RDE responses for the electro-oxidation of 0.1 mol L^{-1} ethanol in 0.1 mol L^{-1} NaOH on the metallopolymer-modified electrode at 500 to 2500 rpm: **black line** = 500 rpm; **red short dot** = 1000 rpm; **blue short dash** = 1500 rpm; and **olive dash dot** = 2500 rpm. Scan rate = 25 mV s^{-1}. **B**) Magnification of the RDE responses in the potential range between 0.30–0.56 V. **C**) Differential curves obtained by RDE data. **D**) Polarization curves for the electro-oxidation of 0.1 mol L^{-1} ethanol in 0.1 mol L^{-1} NaOH on the metallopolymer-modified electrode at 500 to 2500 rpm.

the potential range of 0.46 V–0.56 V vs. SCE slightly decreased (Figure 8B) as a function of the rotation rate. This phenomenon is indicative that the reaction rate does not depend on the access to the bulk reactant but instead depends on the chemisorption rates in the electrocatalytic sites. Presumably, the electrocatalyst surface sites are blocked by hydroxide anion adsorbates and ethanol adsorbates during the first step of nickel(II) oxidation. According to molecular orbital theory, the binding energy of an adsorbate onto a metal cation is largely dependent on the electronic structure of the cation itself.[24] Of particular importance is the presence of an isopotential point at 0.55 V vs. SCE (Figure 8B), i.e., in the potential range where the oxygen evolution reaction occurs. Indeed, the electrode surface may be considered to consist of two independent electrochemical regions; one corresponding to the ethanol electro-oxidation by nickel(IV) and the second corresponding to water oxidation. The two electrochemical processes can be better observed by the differential of the RDE curves (see Figure 8C). The differential current at 0.46 V vs. SCE (electrochemical oxidation of $Ni^{(II)}$) remained quasi-constant independent of the rotation rate. In the potential range of 0.46 V–0.51 V, the diffusion layer thickness significantly influenced the interaction of adsorbed species with the electro-generation of $Ni^{(IV)}$=O and subsequently the electro-oxidation of the intermediate species. Increasing the electrode reaction rate for the oxygen evolution reaction was additionally confirmed by the fact that the initial current shifted to more negative potentials with an increasing rotation rate. In this context, the isopotential point observed in Figure 8B is consistent with a change in the surface state during cycling.

Tafel polarization (applied potential vs. log current density) curves for the metallopolymer-modified electrode have been determined for each rotation rate (extracted from Figure 7A) and are reproduced in Figure 7D. Two linear regions are observed with average Tafel slope values of 246 (±6) mV dec^{-1} for low overpotentials (0.35–0.41 V) and close to 44 (±4) mV dec^{-1} for high overpotentials (0.44–0.47 V). The high Tafel slope at low overpotentials indicates that the rate determining

step is the electrochemical oxidation of nickel(II) with the oxo-bridge formation between metallopolymer columns. Clearly, the decrease of the Tafel slope at high overpotentials is related to a surface with high oxo-bridge coverage. Thus, the EC mechanism is controlled by electron transfer between ethanol and the surface electrode.[25]

The rate constant of the electrocatalytic reaction of the oxidation of ethanol at the surface of the metallopolymer-modified electrode was evaluated by means of chronoamperometry (Figure 9) according to the method of Galus [Eq. (2)]:[26]

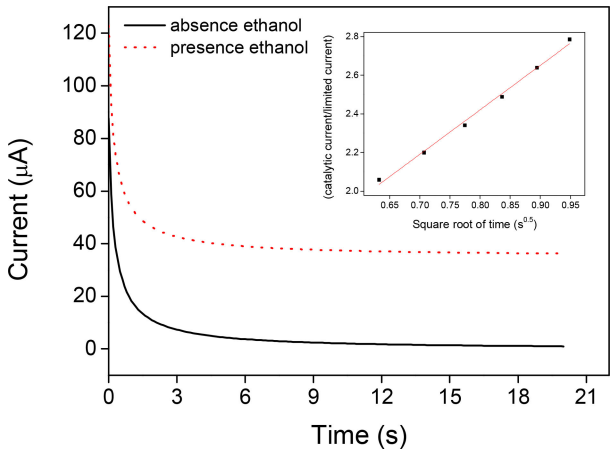

Figure 9. Chronoamperometry curve of ethanol oxidation reaction on the metallopolymer-modified electrode in 0.1 mol L^{-1} NaOH solution: (black line) absence and (red dot) presence of 0.1 mol L^{-1} ethanol. Applied potential = 0.59 V vs SCE. Insert: I_{ox}/I_L versus square root of time.

$$\frac{I_{ox}}{I_L} = \pi^{\frac{1}{2}}(k_{obs}C_0t)^{1/2} \quad (2)$$

where I_{ox} and I_L (amper) are the catalytic and limited currents in the presence and absence of ethanol, respectively. k_{obs} ($mol^{-1}\,s^{-1}$) is the apparent rate constant of oxidation, C_0 (mol L^{-1}) is the concentration of ethanol and t (s) is the elapsed time. For the chronoamperometric analysis, a constant potential of 0.59 V vs. SCE was applied for 20 s at the modified electrode immersed in 0.1 mol L^{-1} ethanol in 0.1 mol L^{-1} sodium hydroxide. From the slope of I_{ox}/I_L versus $t^{1/2}$ plot (insert in the Figure 9), the rate constant of the electrocatalytic reaction of ethanol oxidation was estimated to be approximately 13.61 L $mol^{-1}\,s^{-1}$. Due to a difficulty in determining subproducts and electron transfer number, in the rate of ethanol oxidation was considered by the kinetics of one-electron cross-exchange reaction between the Ni(II)/(III) sites (rate-determining step) and the substrate. The TOF value for the steady-state of catalytic ethanol oxidation[27] at the metallopolymer-modified electrode was calculated to be 1.3 s^{-1} at an overpotential of 200 mV assuming that the rate determining step is the electrochemical oxidation of nickel(II) and all the sites were involved in the electrochemical reaction.

3. Conclusions

The glassy carbon electrode (GC) coated with poly[Ni(α,α′-Me_2 salen)] exhibited an electrocatalytic property toward the ethanol oxidation reaction in NaOH solution. The voltammetric measurements indicated that the metallopolymer acts as an efficient material for the electrocatalytic oxidation of ethanol, where a high-valent nickel(IV) was revealed as the reactive intermediate during the anodic scan. Through the polarization curve, the Tafel slopes were found to be 246 mV dec^{-1} at low overpotentials and 44 mV dec^{-1} at high overpotentials, which suggests that the first electron transfer step is the rate controlling step. An isopotential point was observed in the RDE measurements, revealing that the electrode surface may be considered to consist of two independent electrochemical regions: one corresponding to the ethanol electro-oxidation by nickel(IV) and the second corresponding to the electrocatalytic property for the oxygen evolution reaction. The results are different from the articles with studies of nickel Schiff base complexes,[17,20,28] where nickel(IV) generation was not observed or identified.

Acknowledgments

The authors acknowledge FAPESP (2016/09017-1 and 13/07296-2) and CNPq (3027728/2012-0 and 372986/2011-0) for financial support. SJT. and NSA.

Conflict of Interest

The authors declare no conflict of interest.

Keywords: electro oxidation · fuel cells · heterogeneous catalysis · impedance · metallopolymer

[1] a) C. G. Cameron, P. G. Pickup, *J. Am. Chem. Soc.* **1999**, *121*, 7710–7711; b) B. J. Holliday, T. M. Swager, *Chem. Commun.* **2005**, 23–36; c) G. R. Whittell, M. D. Hager, U. S. Schubert, I. Manners, *Nat. Mater.* **2011**, *10*, 176–188; d) J. C. Eloi, L. Chabanne, G. R. Whittell, I. Manners, *Mater. Today* **2008**, *11*, 28–36.
[2] a) W. J. Liu, W. J. Huang, C. H. Chen, M. Pink, D. Lee, *Chem. Mater.* **2012**, *24*, 3650–3658; b) C. S. Martin, M. F. S. Teixeira, *26th European Conference on Solid-State Transducers, Eurosensor 2012* **2012**, *47*, 1161–1164; c) H. Shiroishi, K. Ishikawa, K. Hirano, M. Kaneko, *Polym. Adv. Technol.* **2001**, *12*, 237–243; d) K. Y. Zhang, S. J. Liu, Q. Zhao, W. Huang, *Coord. Chem. Rev.* **2016**, *319*, 180–195.
[3] P. G. Pickup, *J. Mater. Chem.* **1999**, *9*, 1641–1653.
[4] a) R. Vinoth, S. G. Babu, V. Bharti, V. Gupta, M. Navaneethan, S. V. Bhat, C. Muthamizhchelvan, P. C. Ramamurthy, C. Sharma, D. K. Aswal, Y. Hayakawa, B. Neppolian, *Sci Rep-Uk* **2017**, *7*; b) J. Zhu, *J. Cent. South Univ. Technol. (Engl. Ed.)* **2013**, *20*, 2657–2662; c) L. Fritea, F. Haddache, B. Reuillard, A. Le Goff, K. Gorgy, C. Gondran, M. Holzinger, R. Sandulescu, S. Cosnier, *Electrochem. Commun.* **2014**, *46*, 75–78; d) Y. L. Hou, R. W. Y. Sun, X. P. Zhou, J. H. Wang, D. Li, *Chem. Commun.* **2014**, *50*, 2295–2297.
[5] a) A. Bhunia, P. W. Roesky, Y. H. Lan, G. E. Kostakis, A. K. Powell, *Inorg. Chem.* **2009**, *48*, 10483–10485; b) G. I. Dzhardimalieva, I. E. Uflyand, *J. Coord. Chem.* **2017**, *70*, 1468–1527.
[6] a) M. Li, H. D. Jiao, H. Q. Zhang, S. Q. Jiao, *Int. J. Electrochem. Sci.* **2015**, *10*, 8797–8806; b) J. L. Li, F. Gao, Y. K. Zhang, X. D. Wang, *Chin. J. Polym. Sci.* **2010**, *28*, 667–671; c) S. P. Kumar, K. Giribabu, R. Manigandan, S. Munusamy, S. Muthamizh, A. Padmanaban, T. Dhanasekaran, R. Suresh, V. Narayanan, *Electrochim. Acta* **2016**, *194*, 116–126; d) E. V. Alekseeva, I. A. Chepurnaya, V. V. Malev, A. M. Timonov, O. V. Levin, *Electrochim. Acta* **2017**, *225*, 378–391.

[7] a) C. R. Peverari, D. N. David-Parra, M. M. Barsan, M. F. S. Teixeira, *Polyhedron* **2016**, *117*, 415–421; b) M. T. Nguyen, R. A. Jones, B. J. Holliday, *Macromolecules* **2017**, *50*, 872–883.
[8] C. S. Martin, W. B. S. Machini, M. F. S. Teixeira, *RSC Adv.* **2015**, *5*, 39908–39915.
[9] a) C. S. Martin, T. R. L. Dadamos, M. F. S. Teixeira, *Sens. Actuators B Chem.* **2012**, *175*, 111–117; b) M. F. S. Teixeira, T. R. L. Dadamos, *Procedia Chem.* **2009**, *1*, 297–300; c) T. R. L. Dadamos, M. F. S. Teixeira, *Electrochim. Acta* **2009**, *54*, 4552–4558.
[10] G. A. Shagisultanova, *Teor. Eksp. Khim.* **1991**, *27*, 330–338.
[11] a) L. Chen, L. L. Lu, H. L. Zhu, Y. G. Chen, Y. Huang, Y. D. Li, L. Y. Wang, *Nat. Commun.* **2017**, *8*; b) B. W. Zhang, T. Sheng, Y. X. Wang, X. M. Qu, J. M. Zhang, Z. C. Zhang, H. G. Liao, F. C. Zhu, S. X. Dou, Y. X. Jiang, S. G. Sun, *ACS Catal.* **2017**, *7*, 892–895.
[12] a) S. G. Lemos, R. T. S. Oliveira, M. C. Santos, P. A. P. Nascente, L. O. S. Bulhoes, E. C. Pereira, *J. Power Sources* **2007**, *163*, 695–701; b) M. Li, W. P. Zhou, N. S. Marinkovic, K. Sasaki, R. R. Adzic, *Electrochim. Acta* **2013**, *104*, 454–461; c) L. Assaud, N. Brazeau, M. K. S. Barr, M. Hanbucken, S. Ntais, E. A. Baranova, L. Santinacci, *ACS Appl. Mater. Interfaces* **2015**, *7*, 24533–24542.
[13] a) E. G. Ciapina, S. F. Santos, E. R. Gonzalez, *J. Solid State Electrochem.* **2013**, *17*, 1831–1842; b) R. G. C. S. dos Reis, F. Colmati, *J. Solid State Electrochem.* **2016**, *20*, 2559–2567; c) F. F. Zhang, D. B. Zhou, M. D. Zhou, *J. Energy Chem.* **2016**, *25*, 71–76; d) N. Cantillo, J. Solla-Gullon, E. Herrero, C. Sanchez, *Polymer Electrolyte Fuel Cells 11* **2011**, *41*, 1307–1316.
[14] a) R. K. Pandey, V. Lakshminarayanan, *Appl. Catal. B* **2012**, *125*, 271–281; b) E. Antolini, *Appl. Catal. B* **2010**, *100*, 413–426; c) M. Rosenbaum, U. Schroder, F. Scholz, *J. Solid State Electrochem.* **2006**, *10*, 872–878.
[15] G. A. Shagisultanova, L. P. Ardasheva, *Russ. J. Inorg. Chem.* **2001**, *46*, 352–359.
[16] T. Y. Rodyagina, P. V. Gaman'kov, E. A. Dmitrieva, I. A. Chepurnaya, S. V. Vasil'eva, A. M. Timonov, *Russ. J. Electrochem.* **2005**, *41*, 1101–1110.
[17] N. Wannaprom, P. Vanalabhpatana, *J. Electrochem. Soc.* **2014**, *161*, G86-G97.
[18] a) J. Bisquert, *Electrochim. Acta* **2002**, *47*, 2435–2449; b) J. Bisquert, V. S. Vikhrenko, *Electrochim. Acta* **2002**, *47*, 3977–3988.
[19] a) S. E. Creager, T. T. Wooster, *Anal. Chem.* **1998**, *70*, 4257–4263; b) C. Hortholary, C. Coudret, *C. R. Chim.* **2008**, *11*, 702–708.
[20] N. Kuznetsov, P. X. Yang, G. Gorislov, Y. Zhukov, V. Bocharov, V. Malev, O. Levin, *Electrochim. Acta* **2018**, *271*, 190–202.
[21] a) A. G. Marrani, V. Novelli, S. Sheehan, D. P. Dowling, D. Dini, *ACS Appl. Mater. Interfaces* **2014**, *6*, 143–152; b) L. D'Amario, R. Jiang, U. B. Cappel, E. A. Gibson, G. Boschloo, H. Rensmo, L. C. Sun, L. Hammarstrom, H. N. Tian, *ACS Appl. Mater. Interfaces* **2017**, *9*, 33470–33477; c) S. R. Mellsop, A. Gardiner, A. T. Marshall, *Electrochim. Acta* **2015**, *180*, 501–506; d) *Prog. Inorg. Chem.* **2012**, *57*, 1–591.
[22] M. Pourbaix, *Atlas of electrochemical equilibria in aqueous solutions*, 1st English ed., Pergamon Press, Oxford, New York, **1966**.
[23] Y. J. Leem, K. Cho, K. H. Oh, S. H. Han, K. M. Nam, J. Chang, *Chem. Commun.* **2017**, *53*, 3454–3457.
[24] A. Nilsson, L. G. M. Pettersson, *Chemical Bonding at Surfaces and Interfaces* **2008**, 57–142.
[25] S. Fletcher, *J. Solid State Electrochem.* **2009**, *13*, 537–549.
[26] Z. Galus, *Fundamentals of electrochemical analysis*, Ellis Horwood; Halsted Press, a division of Wiley, Chichester New York, **1976**.
[27] J. M. Saveant, *ChemElectroChem* **2016**, *3*, 1967–1977.
[28] J. B. Raoof, A. N. Golikand, M. Baghayeri, *J. Solid State Electrochem.* **2010**, *14*, 817–822.

Manuscript received: April 25, 2018
Accepted Article published: August 13, 2018
Version of record online: August 28, 2018